Ferroelectricity, Nonlinear Dynamics, and Relaxation Effects in Monoclinic $Sn_2P_2S_6$

Konstantin Z. Rushchanskii,[1,2] Yulian M. Vysochanskii,[1] and Dieter Strauch[2]

[1]*Institute for Solid State Physics and Chemistry, Uzhgorod National University, 54 Voloshyn St., 88000 Uzhgorod, Ukraine*

[2]*Institut für Theoretische Physik, Universität Regensburg, 93040 Regensburg, Germany*

(Received 15 March 2006; published 16 November 2007)

An *ab initio*–based model of the temperature-induced ferroelectric phase transition in $Sn_2P_2S_6$ (SPS) as a prototype of an unconventional ferroelectric is developed. The order parameter in SPS is found as the valley line on a total-energy surface of the zone-center fully symmetrical A_g and polar B_u distortions. Significant nonlinear coupling between order parameter and strain is observed. Monte Carlo simulations describe the additional low-temperature rearrangement in polar structure, which appears in domain boundaries, and describe the relaxation phenomena near the ferroelectric phase transition.

DOI: 10.1103/PhysRevLett.99.207601 PACS numbers: 77.84.−s, 71.15.Mb, 77.80.Bh

Over the years, the ferroelectric perovskites have been extensively studied from both the experimental and theoretical points of view. The most important example is $BaTiO_3$ [1]. Because of its simple crystal structure, the first-principles scheme based on the local-mode approach was developed and successfully applied to the study of the ferroelectric phase transition (PT) more than ten years ago [2]. In the present work we investigate the peculiarities of chalcogenide-containing ferroelectrics, a wide class of low-symmetry compounds, where the strongly pronounced nonlinear phenomena have two origins: (i) The polarizability of the anion sublattice is much higher than in oxides; (ii) the symmetry is lower, allowing effects which are forbidden in the high-symmetry perovskite structures.

One example of this class of ferroelectrics is the monoclinic ditin-hexathiophosphate $Sn_2P_2S_6$ (SPS), a prospective material for fast holography and nonlinear optics in the infrared region [3]. The unit cell of SPS contains 2 formula units, i.e., 20 atoms, forming anionic complexes $(P_2S_6)^{4-}$ with predominantly covalent bonding and ferroelectric-active Sn^{2+} cations, connected via ionic bonding to the anion complexes [4,5]. From a fundamental point of view many interesting phenomena such as two-length scale critical behavior [6], coexistence of NMR resonances of paraelectric (PE) and ferroelectric (FE) phases [7], non-Debye dielectric dispersion near 60 K [8], relaxation processes near the second-order PT at 337 K [9], displacive vs order-disorder crossover [10], complex nature of the optic soft mode in the FE phase, and nonlinear soft-mode interactions in the PE phase [11–14] have been observed experimentally in this proper uniaxial ferroelectric. Isostructural to the SPS, the $Sn_2P_2Se_6$ ferroelectric exhibits an incommensurate phase between the PE and FE phases [15]. The $Sn_2P_2(Se_xS_{1-x})_6$ solid solutions have a rare Lifshitz point in the T, x phase diagram [15], where an incommensurate phase appears.

The aim of this Letter is to report a reasonable microscopic model for SPS ferroelectrics with a *monoclinic* reference structure. The monoclinic structure was recently studied in $Pb(Zr, Ti)O_3$ using *ab initio* methods for the *cubic* reference structure utilizing the effective-Hamiltonian approach for nonzero temperature investigations [16], and analytical interatomic potentials for studies of compositional disordering [17]. We will point out that, in contrast to $BaTiO_3$ and $PbTiO_3$ [18], the FE instability in SPS arises from nonlinear interaction of polar and fully symmetrical modes, which leads to a triple-well potential. We will present theoretical results, describing the conjectured structural disorder with the polar symmetry [8] as a reconstruction in the domain boundaries, and coexistence of NMR resonances of PE and FE phases near the PT [7] due to triple-well potential-energy surface.

We pursue a completely *ab initio* effective-Hamiltonian approach [2] to carry out a theoretical study of the FE phase transition in SPS, since (i) the transition from the high-symmetry $P2_1/n$ to the low-symmetry Pn structure can be described in terms of small structural distortions [4,5], and (ii) the polar soft mode with B_u symmetry in the PE phase is clearly observed experimentally [13,14]. Our first-principles calculations of the Born effective charges, phonon spectra, and elastic properties have been conducted within the density functional perturbation theory using the ABINIT code [19] and the pseudopotential method [20] with the following electronic configurations of the pseudoatoms: $5s^25p^2$ for Sn, $3s^23p^3$ for P, and $3s^23p^4$ for S. The exchange-correlation interaction was taken into account within the local-density approximation (LDA) [21]. We have used a $4 \times 4 \times 4$ **k**-point mesh, and a plane-wave energy cutoff of 30 Ry. The theoretical values of the structural parameters differ from the experimental ones [4,5] within 1% for the P–P and P–S interatomic distances and within 9% for Sn–S.

Our finite-temperature studies of the PT proceeds in four steps: (i) investigation of the transition path to determine the important degrees of freedom, (ii) recasting the full anharmonic lattice Hamiltonian into a form with a reasonably small number of parameters, (iii) determination of the parameters from the highly accurate *ab initio* LDA calculations, and (iv) Monte Carlo (MC) simulations to determine the phase-transformation behavior of SPS.

In $BaTiO_3$ and other perovskites the subspace of the important degrees of freedom for the anharmonic part of the Hamiltonian is determined by just the eigenvector of the soft mode, which has imaginary frequency in harmonic *ab initio* phonon calculations. In contrast, we have found that in the case of SPS the phonon spectrum of the high-symmetry phase is dynamically stable over the entire range of the Brillouin zone. Compatible with the PT group-subgroup relation are two mode types: polar B_u and non-polar fully symmetrical A_g. Using the resulting relaxed geometry of the PE and the FE phases and the zone-center normal-mode displacements in the PE phase we can decompose the reference PE structure distortions in terms of the A_g and B_u optical-mode amplitudes. It turned out that the B_u (39 cm^{-1}) and A_g (41 cm^{-1}) modes with the lowest energy make the largest contributions to the FE lattice distortions, but the contributions of the other modes with a higher energy cannot be neglected as well. The eigenvector of the low-energy optical B_u mode describes in-phase displacements of the four Sn^{2+} cations mostly along the **a**-axis and the corresponding counter-phase displacements of the two anion complexes. In the low-energy A_g vibration only the out-of-phase displacements in the cation sublattice are observed. These findings are very similar to the recent semiempirical results [22].

Frozen-phonon calculations of the total energy for the low-energy B_u mode does not point at any additional minima, which might be related to the FE instability. But surveying the potential-energy surface in the subspace of low-energy B_u and A_g modes the strong deviation from harmonic behavior can be clearly seen, though the global FE minima still are not observed (see Fig. 1). The energy positions of the FE *global* minima can be reached only in the subspace of *all* $15A_g + 13B_u$ normal coordinates and four monoclinic components of strain, the order parameter is determined as a valley line in the 32-dimensional phase space. Using the approach proposed in [23], we evaluate the total energy as a function of an amplitude $u = (u_x^2 + u_y^2 + u_z^2)^{1/2}$ of the FE atomic displacements $u_\alpha = [\sum_n (r_\alpha^{n(p)} - r_\alpha^{n(PE)})^2]^{1/2}$ in the PE unit cell, where $\mathbf{r}^{n(PE)}$ and $\mathbf{r}^{n(p)}$ are the position of atom n in the PE and polar structures, respectively. For each u we have performed the simulations of (i) the direct-path, obtained with no structural relaxations connecting PE and FE configurations, (ii) the internal relaxation path, when the internal degrees of freedom were allowed to relax, while the lattice shape was fixed to the reference PE structure, and (iii) the real path, when all possible degrees of freedom were allowed to relax during energy minimization procedure. For the first two simulations the homogeneous strain induced by internal deformation was relaxed using linear stress-strain relation with calculated clamped-ion elastic moduli, and the related elastic energy was extracted from the corresponding path. The results are collected in Fig. 2.

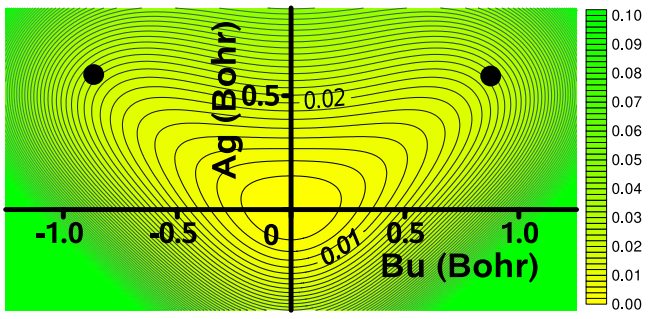

FIG. 1 (color online). Frozen-phonon energy surface (in eV) for a linear combination of A_g and B_u mode amplitudes for $Sn_2P_2S_6$ within LDA. Black circles denote the projections of the positions of the global FE minima.

The obtained energy profile has a triple-well shape, where two FE valleys arise from the nonequivalent lattice distortions $Ag \pm B_u$ as a result of strong nonlinear $A_g B_u^2$ interaction. The PE valley is the main source of the experimentally observed [11,13,14] relaxation part of the order-parameter fluctuation spectrum. Relaxation processes, observed as the coexistence of the FE and PE NMR-resonances within a 16 K temperature range below the PT [7], also confirm the obtained triple-well shape of the potential-energy surface.

In the vicinity of the PE reference structure a difference between the real path and the elastically relaxed counterparts for the direct path and the internal relaxation path is considerably large (see Fig. 2), which indicates a significant nonlinear coupling between the order parameter and the strain. The internal relaxation path coincides well with the real path only in the middle of the valley line, while its elastically relaxed counterpart does not reach the global FE minima in the FE valley. Within the whole of the FE valley the real path coincides with the elastically relaxed counterpart of the direct path. Therefore, as a local polar distortion we have chosen the set of the linear atomic displacements

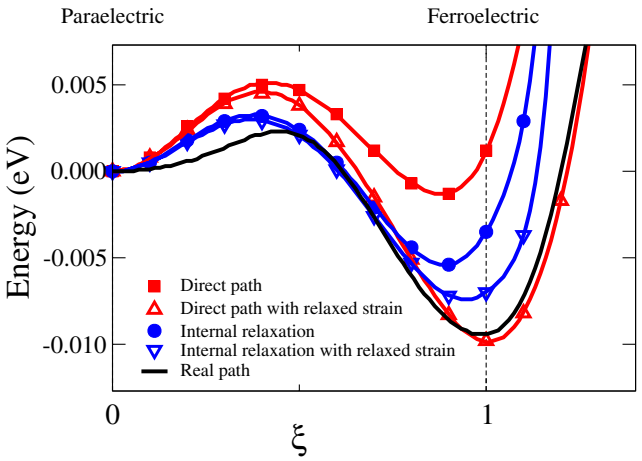

FIG. 2 (color online). Energy profile along the valley lines in $Sn_2P_2S_6$ within LDA.

with reduced amplitude $\xi = u/u^{FE}$ along the direct path. This distortion accounts for *all* 28 optical A_g and B_u modes only implicitly, while the coupling with four elastic deformations is treated explicitly. The displacement of the atom n from its position in the PE structure, multiplied by the respective value of the Born effective charge, calculated for the reference PE phase, is associated with the elementary electric dipole $\boldsymbol{\mu}_n$, contributing to the polarization of the unit cell. The linear dependence of the atomic displacements with respect to the distortion amplitude ξ allowed us to construct the effective Hamiltonian in the simple pseudospin form, similar to Ref. [2]:

$$E^{\text{tot}} = \sum_i \sum_{k=1}^{8} A_k \xi_i^{2k} + \sum_i \xi_i \sum_{l\in(x,y,z)} B_l[\xi_{i+l} + \xi_{i-l}] + \frac{1}{2\epsilon_\infty^*} \sum_{i,j} \sum_{m,n=1}^{20} \sum_{\mathbf{d}} \frac{\boldsymbol{\mu}_m \cdot \boldsymbol{\mu}_n - 3(\boldsymbol{\mu}_m \cdot \hat{\mathbf{D}})(\boldsymbol{\mu}_n \cdot \hat{\mathbf{D}})}{|\mathbf{D}|^3} \xi_i \xi_j + \frac{1}{2} V_c \sum_{a,b} C_{ab} \varepsilon_a \varepsilon_b + V_c \sum_i \sum_a \sigma_a(\xi_i) \varepsilon_a,$$

where the sums over i and j run over all unit cells within the simulation MC cell; the sum over l runs over the unit cells neighboring to the i cell in the x, y, and z directions; the sums over m and n run over all elementary dipoles $\boldsymbol{\mu}$ within the unit cell; $\mathbf{D} = (\mathbf{R}_i - \mathbf{R}_j) - (\mathbf{r}^m - \mathbf{r}^n) + \mathbf{d}$, where $\mathbf{R}_i$ is the position of the unit cell i, $\mathbf{r}^n$ is the position of the elementary dipole $\boldsymbol{\mu}_n$ within the unit cell, and $\mathbf{d}$ is the position of the simulation cell replicas in the system with periodic boundary conditions. The use of the polynome with eight A_k constants is necessary to properly describe the anharmonicity of the local-distortion self-energy (see the curve "Direct path" in Fig. 2). The other input parameters for the effective Hamiltonian are the following: three B_l constants, describing the short-range nearest-neighbor intersite coupling; one ϵ_∞^* constant calculated as a trace of the optical dielectric tensor; four monoclinic lattice parameters, describing the geometry and volume V_c of the MC cell; twelve independent constants of the clamped-ion elastic tensor C_{ab}, and four dependencies $\sigma_a(\xi)$ of the stress, induced by the internal deformation ξ. Computational details and the values of the parameters can be found in [24].

We solve this Hamiltonian using the METROPOLIS MC simulations [25] on an $L \times L \times L$ supercell with artificial periodic boundary conditions. As usual [2], we choose the single-flip algorithm and define one MC sweep as L^3 flip attempts. It is well known that the ferroelectric PT temperature is very sensitive to the hydrostatic pressure [2]. Since within LDA the equilibrium volume of the PE phase is underestimated, the calculated PT temperature $T = 100$ K for $Sn_2P_2S_6$ differs significantly from the experimental value $T = 337$ K. Therefore, as usual [2], the negative-pressure correction has been applied. We have found good agreement with the experimental PT temperature for the external pressure of $P = -4.2$ GPa, which is of the same order as for perovskites [2]. With this correction the difference between the theoretical and experimental volume at low temperature is within 1.5%. We have used 10^4 and 4×10^4 MC sweeps for equilibration and production, respectively. A typical value of the MC cell was $L = 12$. Using a larger box with $L = 14$ and $L = 20$ slightly shifts the PT temperature upwards, but does not influence the main peculiarities of the PT.

In accordance with the experimental observations [15], our model describes the existence of FE 180° domain ordering along the **b**-axis. No additional boundary conditions were applied for the pseudospins localized at the domain wall, and the quantum effects at low temperatures were neglected. We performed two runs in heating ($T = 4$–350 K) and cooling ($T = 130$–4 K) mode with temperature steps of 2 K. For both runs an initial configuration has been chosen with the domain boundary as shown in Fig. 3(a), left, but with equal within domain-space values of pseudospins $\pm P_s$, which correspond to the FE minimum and determine the saturated values of the possible spontaneous polarization P_s.

After the equilibration run in the heating mode the domain boundary becomes smooth, leading to the multipeak distribution associated with the two types of pseudospins [see Fig. 3(a)]: (i) sharp peaks for $\pm P_s$ pseudospins, and (ii) broad peaks for $\pm \frac{1}{2} P_s$, which correspond to the pseudospins near the domain boundaries (see left panel). Heating leads to the strong decrease of the type-(i) peaks and to significant smoothing of the type-(ii) peak distribution. This configuration survives up to 66 K, where the

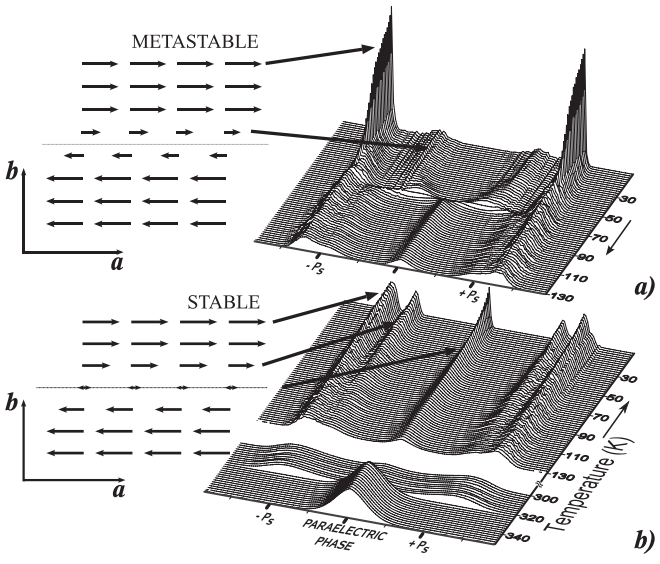

FIG. 3. Left: Snapshots of pseudospin configurations near the domain boundaries (thin line) for (a) metastable and (b) stable ordering. Right: Corresponding average histograms of pseudospin distribution vs temperature from MC simulations ($L = 12$; 40 000 MC sweeps per temperature point).

pseudospin distributions transform to a three-peak form [see Fig. 3(b)]: (i) peaks for $\pm P_s$; (ii) peaks near $\pm \frac{3}{4} P_s$, related with the domain boundaries, and (iii) at $P_s = 0$, representing the existence of the nonpolar cells at the domain boundaries. This pseudospin configuration is more stable, having a free energy lower by about 1 meV (per unit cell) at $T = 4$ K and 10 meV at $T = 60$ K surviving down to $T = 324$ K, where the transition to the PE phase occurs. Upon cooling the initial configuration with a sharp domain boundary changes into the three-peak form with a central peak in the distribution after the equilibration run at $T = 130$ K. This configuration is maintained down to $T = 4$ K and reveals the sharpening of the peak distribution. So, we observe the presence of a metastable configuration of pseudospins, which can be conserved in the temperature range of less than 65 K. The rearrangement occurs in the domain-wall region, and it is related to the presence of nonpolar cells at the boundary as a direct consequence of the triple-well potential. This can be responsible for the experimentally observed non-Debye type dielectric dispersion at low temperatures near $T = 60$ K [8], which was suggested to be related to the structural disordering in the polar phase. Above $T = 60$ K thermal fluctuations allow the motion of the domain-walls changing their shape from stable configuration to the metastable one. At low temperatures an external electric field can stabilize the metastable configuration and hence fix the smooth shape of the domain boundary by decreasing the amount of $P_s = 0$ pseudospins. This in turn leads to the freezing of the contribution of domain-wall motions to the macroscopic polarization, which is observed experimentally. Note that the calorimetric experiments [10], which are conducted at equilibrium conditions, reveal no anomalies in the low-temperature region. The same results (not presented here) were obtained for the $L \times 4L \times L$ MC cell, enlarged along the **b**-axis as well as for the isostructural selenide $Sn_2P_2Se_6$.

In conclusion, we have presented the successful application of the local-mode approach to the low-symmetrical monoclinic chalcogenide ferroelectrics. We have found a complex potential-energy surface, leading to the freezing phenomena at low temperatures and to the existence of nonpolar cells in the ferroelectric phase. The nonlinear mode interactions lead to a triple-well shape of the potential-energy surface as a result of significant electron-phonon interaction and, correspondingly, to the theoretically and experimentally observed complex nature of the soft mode. We believe this nonlinearity to be a reflection of the strong polarizability of Sn^{2+} cations in chalcogenide surrounding, which will be a subject of a forthcoming article.

K. Z. R. is grateful to the Alexander von Humboldt Foundation for financial support.

[1] M. E. Lines and A. M. Glass, *Principles and Applications of Ferroelectrics and Related Materials* (Clarendon, Oxford, 1997).
[2] W. Zhong, D. Vanderbilt, and K. M. Rabe, Phys. Rev. B**52**, 6301 (1995).
[3] M. Jazbinšek, G. Montemezzani, P. Günter, A. A. Grabar, I. M. Stoika, and Y. M. Vysochanskii,J. Opt. Soc. Am. B **20**, 1241 (2003).
[4] G. Dittmar and H. Schaefer, Z. Naturforsch., B **29**, 312 (1974).
[5] B. Scott, M. Pressprich, R. D. Willet, and D. A. Cleary, J. Solid State Chem. **96**, 294 (1992).
[6] J. Hlinka, R. Currat, M. de Boissieu, F. Livet, and Y M. Vysochanskii, Phys. Rev. B **71**, 052102 (2005).
[7] X. Bourdon, A.-R. Grimmer, A. Kretschmer, and V. B. Cajipe, in *Proceedings of the 30th Congress Ampere on Magnetic Resonance and related Phenomena*, edited by A. F. Martins, A. G. Feigo, and J. G. Moura (FCT/UNL, Lisbon, 2002).
[8] M. Iwata, A. Miyasita, Y. Ishibashi, K. Moriya, and S. Yano, J. Phys. Soc. Jpn. **67**, 499 (1998).
[9] V. Samulionis, J. Banys, and Y. M. Vysochanskii, Ferroelectrics **257**, 135 (2001).
[10] K. Moriya, H. Kuniyoshi, K. Tashita, Y. Ozaki, S. Yano, and T. Matsuo, J. Phys. Soc. Jpn. **67**, 3505 (1998).
[11] A. V. Gomonnai, Y. M. Vysochanskii, A. A. Grabar, and V. Y. Slivka, Sov. Phys. Solid State **23**, 2105 (1981).
[12] A. V. Gomonnai, Y. M. Vysochanskii, and V. Y. Slivka, Sov. Phys. Solid State **24**, 606 (1982).
[13] S. W. H. Eijt, R. Currat, J. E. Lorenzo, P. Saint-Grégoire, S. Katano, T. Janssen, B. Hennion, and Y. M. Vysochanskii, J. Phys. Condens. Matter **10**, 4811 (1998).
[14] S. W. H. Eijt, R. Currat, J. E. Lorenzo, P. Saint-Grégoire, B. Hennion, and Y. M. Vysochanskii, Eur. Phys. J. B **5**, 169 (1998).
[15] Y. M. Vysochanskii and V. Y. Slivka, Sov. Phys. Usp. **35**, 123 (1992).
[16] L. Bellaiche, A. Garcia, and D. Vanderbilt, Phys. Rev. Lett. **84**, 5427 (2000).
[17] I. Grinberg, V. R. Cooper, and A. M. Rappe, Nature (London) **419**, 909 (2002).
[18] R. E. Cohen, Nature (London) **358**, 136 (1992).
[19] X. Gonze, J.-M. Beuken, R. Caracas, F. Detraux, M. Fuchs, G.-M. Rignanese, L. Sindic, M. Verstraete, G. Zerah, F. Jollet, Comput. Mater. Sci. **25**, 478 (2002).
[20] N. Troullier and J. L. Martins, Phys. Rev. B **43**, 1993 (1991).
[21] J. P. Perdew and Y. Wang, Phys. Rev. B **33**, 8800 (1986).
[22] M. B. Smirnov, J. Hlinka, and A. V. Solov'ev, Phys. Rev. B **61**, 15 051 (2000).
[23] T. Hashimoto, T. Nishimatsu, H. Mizuseki, Y. Kawazoe, A. Sasaki, and Y. Ikeda, Jpn. J. Appl. Phys.**43**, 6785 (2004).
[24] K. Z. Rushchanskii, Y. M. Vysochanskii, and D. Strauch (to be published).
[25] N. Metropolis, A. W. Rosenbluth, M. N. Rosenbluth, A. H. Teller, and E. Teller, J. Chem. Phys. **21**, 1087 (1953).